# Multi-sensor anomalous change detection at scale

Amanda Ziemann, Christopher X. Ren, and James Theiler

Intelligence and Space Research, Los Alamos National Laboratory, Los Alamos, NM 87545

## ABSTRACT

Combining multiple satellite remote sensing sources provides a far richer, more frequent view of the earth than that of any single source; the challenge is in distilling these petabytes of heterogeneous sensor imagery into meaningful characterizations of the imaged areas. To meet this challenge requires effective algorithms for combining heterogeneous data to identify subtle but important changes among the intrinsic data variation. The major obstacle to using heterogeneous satellite data to monitor anomalous changes across time is this: subtle but real changes on the ground can be overwhelmed by artifacts that are simply due to the change in modality. Here, we implement a joint-distribution framework for anomalous change detection that can effectively "normalize" for these changes in modality, and does not require any phenomenological resampling of the pixel signal. This flexibility enables the use of satellite imagery from different sensor platforms and modalities. We use multi-year construction of the Los Angeles Stadium at Hollywood Park (in Inglewood, CA) as our testbed, and exploit synthetic aperture radar (SAR) imagery from Sentinel-1 and multispectral imagery from both Sentinel-2 and Landsat 8. We explore results for anomalous change detection between Sentinel-2 and Landsat 8 over time, and also show results for anomalous change detection between Sentinel-1 SAR imagery and Sentinel-2 multispectral imagery.

**Keywords:** change detection, anomalous change detection, multispectral imagery, synthetic aperture radar, multi-sensor, multi-modal

## 1. INTRODUCTION

The remote material discrimination enabled by spectral remote sensing naturally lends itself to the following questions: if I have one or more images of a given scene, what has changed? Furthermore, where are the changes that are interesting? One analyst might, for example, be interested in seasonal variations from summer to autumn that result in drier vegetation. Another analyst might not care about broader seasonal changes, but might be interested in a building that is constructed during that time.[1–3] Both of these circumstances will result in true spectral changes, and so the challenge then becomes this: how do we translate the arguably subjective and certainly application-dependent concept of an "interesting change" to an objective mathematical framework that can be used to exploit remote sensing images? An initial step is to make the distinction between image-wide pervasive differences and rare anomalous changes. The paradigm of anomalous change detection (ACD),[4–11] which is grounded in concepts from anomaly detection,[12–16] seeks to identify *changes that are different from how everything else might have changed.* This borrows from the classic anomaly detection framework, which attempts to characterize that which is "typical" and then uses that to identify deviations from what is expected or common.

Anomalous change detection approaches have historically (and sensibly) assumed that the images come from the same sensor, and as as a result have the same spectral channels. This is particularly important for frameworks that use some sort of a difference image, as that requires the two images to be in the same domain. As airborne and spaceborne remote sensing becomes increasingly more accessible, however, the variety of sensor designs and modalities is growing dramatically. The development of a flexible and sensor-agnostic change detection approach allows for continuous exploitation of *all* imagery over a particular area, without having to wait for the same sensor to revisit that area.

Contact: {ziemann; cren; jt}@lanl.gov

### 1.1 Anomalous Change Detection

The most obvious way to find differences in a pair of images is to literally take the difference: to subtract the images, and look for pixels where that difference is large or in some other way interesting or unusual. Indeed, traditional change detection algorithms (such as Change Vector Analysis[17–20]) are based on analyzing the vector-valued differences at each pixel. One of the difficulties with this approach is that these differences may be dominated by environmental factors (atmospheric transmission, aerosol scattering, solar illumination, view angle, sensor characteristics, etc.) that vary from acquisition to acquisition. The difficulties become truly problematic when the two images are acquired by different sensors, possibly over a different range of wavelengths, or even different phenomenologies. When the number of bands is different, then it is not just a bad idea to subtract them, it is a mathematical impossibility.

The idea behind transformation-based anomalous change detection is to in some way equalize the images so that pervasive differences are suppressed and, at the same time, salient changes are maintained or enhanced; this can be done in a physics-driven way[21, 22] or a data-driven way.[4–7] The chronochrome algorithm of Schaum and Stocker[4] is a simple and effective anomalous change detector, providing a good illustrative example of data-driven equalization. To that end, consider a pair of spatially-corresponding pixels from two images of a scene taken at different times, and let $\mathbf{x}$ and $\mathbf{y}$ represent their spectra. A matrix $L$ is derived so that $\hat{\mathbf{y}} = L\mathbf{x}$ is a good approximation to $\mathbf{y}$ for most of the pixels in the scene ($L$ is sometimes called a "predictor"). In particular, $L$ is chosen to minimize the average of $\|\mathbf{y} - L\mathbf{x}\|^2$ over the whole image. Now, the vector quantity $\mathbf{y} - L\mathbf{x}$ will be relatively small over most of the image (after all, $L$ was chosen to minimize its average magnitude). But for anomalously changed pixels, that vector difference will be of larger magnitude. In the algorithm, the scalar anomalousness score is given by the Mahalanobis magnitude of the vector-valued *difference*. Note that the effect of $L$ is to provide a data-driven equalization in making $L\mathbf{x}$ as much like $\mathbf{y}$ as possible. There is no need for $L$ to be square, so this works even when the number of bands in the two images is different. Various chronochrome extensions have been made, including adapting it to a target detection framework where changes are used to characterize the target-free background at any given pixel.[23, 24]

## 2. JOINT-DISTRIBUTION ACD METHODOLOGY

In the distribution-based approach, introduced in Ref. [25], there is no subtraction at all. In this formulation, we begin with a joint distribution $P(\mathbf{x}, \mathbf{y})$ that describes a typical pair of co-registered pixels $\mathbf{x}$ and $\mathbf{y}$ taken from the two images of interest. Following the usual prescription from anomaly detection, we *could* take our anomalies to be points for which $P(\mathbf{x}, \mathbf{y})$ is small, but this would go after anomalous pairs of pixels and in doing so would find straight anomalies in addition to anomalous changes. To focus in on just the unusual *changes*, we define a nonuniform "background distribution" $Q(\mathbf{x}, \mathbf{y}) = P(\mathbf{x})P(\mathbf{y})$ where

$$P(\mathbf{x}) = \int P(\mathbf{x}, \mathbf{y}) \mathrm{d}\mathbf{y}, \tag{1}$$

$$P(\mathbf{y}) = \int P(\mathbf{x}, \mathbf{y}) \mathrm{d}\mathbf{x}. \tag{2}$$

Here, $Q(\mathbf{x}, \mathbf{y})$ describes "normal" points exhibiting anomalous changes. By contrast, $P(\mathbf{x}, \mathbf{y})$ describes normal points exhibiting normal changes. That is because $P(\mathbf{x}, \mathbf{y})$ describes the data, and the statistics of our data are what we use to define normal. The key notion behind this distribution-based approach is to consider the ratio of these two likelihoods:

$$\frac{P(\text{normal points exhibiting anomalous changes})}{P(\text{normal points exhibiting normal changes})} = \frac{P(\mathbf{x})P(\mathbf{y})}{P(\mathbf{x}, \mathbf{y})}. \tag{3}$$

And as a practical matter it is useful to take the logarithm (which is merely a monotonic rescaling of the values), so we can define

$$\mathcal{A}(\mathbf{x}, \mathbf{y}) = \log \frac{P(\mathbf{x})P(\mathbf{y})}{P(\mathbf{x}, \mathbf{y})} \tag{4}$$

$$= \log P(\mathbf{x}) + \log P(\mathbf{y}) - \log P(\mathbf{x}, \mathbf{y}). \tag{5}$$

The functional form of this expression allows us to interpret the anomalousness as a mutual information between the pixels $\mathbf{x}$ and $\mathbf{y}$. We remark that when the distribution is Gaussian, then the contours of constant anomalousness (that is, the boundaries between what is normal and what is anomalous) are hyperbolic. This motivates the name Hyperbolic Anomalous Change Detection (HACD). We focus here on HACD, but there are other variants such as EC-HACD, where the distributions are elliptically-contoured,[26] and there has been research into using parametric distributions,[27] kernelized distributions,[28] spatio-spectral distributions,[29] and sequences of images.[30,31] The implementation of HACD used here employs local co-registration adjustment (LCRA) for increased robustness to potential misregistration issues.[32,33] Because HACD does not use a channel-by-channel comparison between pixels, but rather compares pixel distributions, the approach is sensor agnostic; it only requires that the two images be sampled to the same spatial domain.

## 3. EXPERIMENTS

To investigate the feasibility of anomalous change detection for multi-sensor scenarios, we applied HACD to remote sensing images taken from a variety of satellite-based sensors: Sentinel-1 (SAR), Sentinel-2 (MSI), and Landsat 8 (MSI).

### 3.1 Testbed and Satellite Sensors

In 2016, ground broke on Los Angeles Stadium at Hollywood Park, the working name for the open air stadium and entertainment complex currently under construction (at the time of publication) in Inglewood, CA.[34] The stadium is scheduled to be completed in 2020 and will be the home arena for both the Los Angeles Rams and the Los Angeles Chargers of the National Football League. The spatial footprint of the stadium is 298 acres, and it lies at the following coordinates: 33.95345°N, 118.3392°W. The timeframe and spatial scale of this construction site make it a useful test bed for developing, implementing, and exploring the results of distribution-based anomalous change detection across multiple sensors and temporal scales. We do not have explicit ground truth masks, but we use visual inspection (and occasionally, as noted below, archived news stories and historical Google Earth imagery) to identify changes that we can qualitatively compare to our results.

We used public domain satellite imagery for this study, and all sensors were global-coverage systems (as opposed to tasking-based); this access to reliable and repeatable historical imagery collections is crucial for looking at changes over time. In particular we used imagery from the European Space Agency (ESA) Copernicus program,[35] namely SAR imagery collected by Sentinel-1 and MSI collected by Sentinel-2. We also used MSI from Landsat 8, the United States Geological Survey (USGS) and NASA satellite.[36] Specific details about the satellites and their sensors are provided in Fig. 1. Of note is that Sentinel-1 is a first-of-its-kind system as a global-coverage public domain SAR satellite, providing a number of new research opportunities, *e.g.*, SAR-to-SAR change detection.

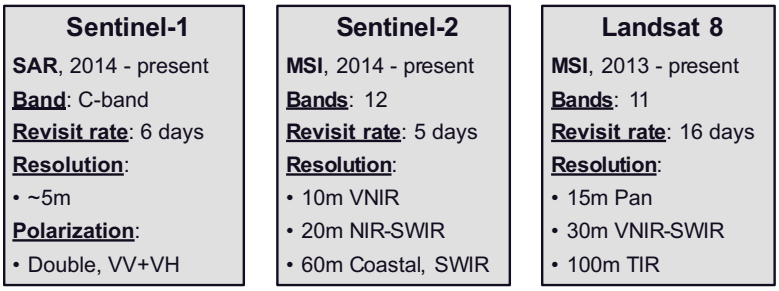


Figure 1. Sensor specifications for Sentinel-1, Sentinel-2, and Landsat 8.

### 3.2 MSI to MSI: Sentinel-2 and Landsat 8

For our first experiment, we looked at changes in images from different sensors within the same modality (multi-spectral). Using Sentinel-2 and Landsat 8 images, we analyzed a 1500 m × 1500 m area including and surrounding

the stadium, and broke it into 9 subtiles (see Fig. 2). We pulled all Sentinel-2 and Landsat 8 images over a 1.5-year period, kept the relatively cloud-free images, and derived ACD maps for every consecutive pair of images (effectively using a sliding temporal window); we then computed summary statistics on the results within each subtile. Nearest neighbor resampling was used to spatially sample the images so they were all at 10 m resolution. As was noted in Section 2, no spectral resampling was needed even though the number of bands and bandwidths varied between the two sensors.


Figure 2. The nine subtiles in the stadium area that were used to track changes between Landsat 8 and Sentinel-2 over a 1.5-year period. Each subtile covers 500 m × 500 m.

### 3.3 SAR to MSI: Sentinel-1 and Sentinel-2

For our second experiment, we analyzed an image pair from different sensors *across different modalities*. We looked at a 2500 m × 2500 m area including and surrounding the stadium, and purposely picked images that were far apart in time (with "Image 1" occurring prior to construction) so that there would be a large change between them. As a baseline, we looked at changes between a Sentinel-2 image from Dec. 2015 and a Sentinel-2 image from Mar. 2019 (the associated RGB composites are shown in Fig. 3). Then, we looked at changes between a Sentinel-1 SAR image from Dec. 2015 and the same Sentinel-2 image from Mar. 2019 (as shown in Fig. 4).

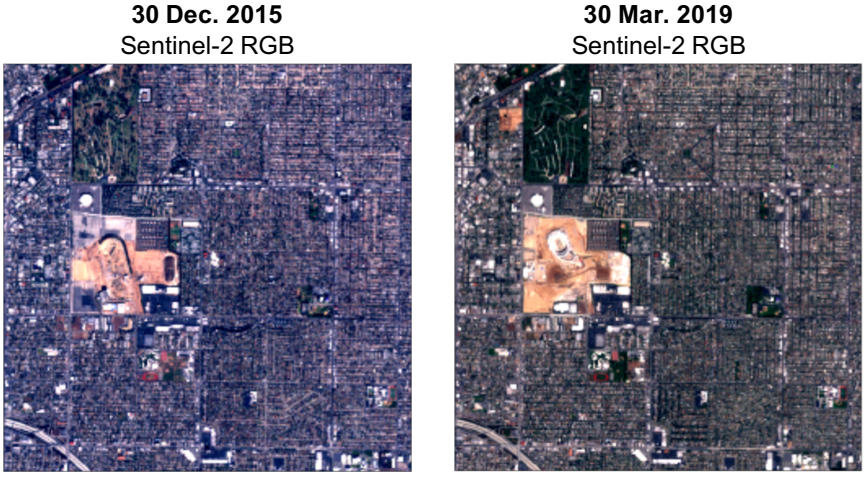


(a) (b)

Figure 3. Color composites of the Sentinel-2 images used for baseline ACD results. The multispectral Sentinel-2 image has 12 bands and the color images shown here are constructed from the red, green, and blue bands.

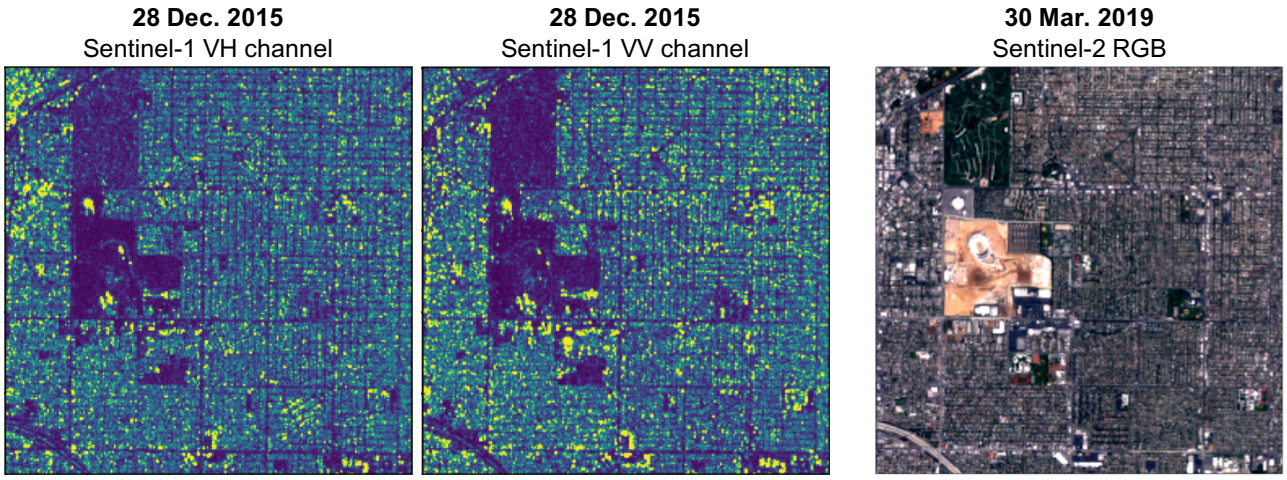


(a) (b)

Figure 4. Color composites of the Sentinel-1 and Sentinel-2 images used for cross-modality ACD analysis. Note that each channel of the Sentinel-1 image is grayscale, though it is displayed here with a color scale that spans blue to green to yellow, with lighter color corresponding to higher SAR amplitude. The multispectral Sentinel-2 image has 12 spectral bands; the color image shown here is constructed from the red, green, and blue bands.

## 4. RESULTS

We review the results of our two main experiments: the first looks at changes between Sentinel-2 and Landsat 8 MSI throughout a 1.5-year period, and the second looks at changes between Sentinel-1 SAR imagery and Sentinel-2 MSI.

### 4.1 MSI to MSI: Sentinel-2 and Landsat 8

The results of our first experiment, where we looked at continuous anomalous change detection results across Sentinel-2 and Landsat 8 images collected throughout a 1.5-year period, are shown in Fig. 5. The plot at the top shows the maximum ACD value within each subtile over time, and for exploration we focus in on three of the higher ACD scores (labeled A, B, and C). Every point in the plot is derived from some consecutive pair of Sentinel-2 and Landsat 8 images (not necessarily in that order).

The images associated with *anomalous change A* are a Sentinel-2 image from 17 Aug. 2017 and a Landsat 8 image from 28 Aug. 2017. The highlighted region (red box) in Subtile 0 is where the high-valued anomalous change occurred. The white circular region directly to the left of the anomalous change is The Forum, an indoor arena that often holds large events. The anomalous change appears to be mobile, so we looked into events at The Forum around these dates. It turns out that on 27 Aug. 2017, The Forum hosted the MTV Video Music Awards; the anomalous change likely corresponds to trucks or caravans associated with the awards show.[37]

The images associated with *anomalous change B* are a Landsat 8 image from 28 Jun. 2018 and a Sentinel-2 image from 13 Jul. 2018. The highlighted region in Subtile 0 is where the high-valued anomalous change occurred. This region is over the main part of the construction site (surrounding the actual stadium), and corresponds to ongoing construction changes.

The images associated with *anomalous change C* are a Landsat 8 image from 16 Sept. 2018 and a Sentinel-2 image also from 16 Sept. 2018. This change appears in the RGB composite image as an elongated red and green and blue streak; we suspect that it is an airplane flying over the scene as the satellite was taking the image. Because of the pushbroom nature of the satellite imager, the red and green and blue components for a given position on the ground are imaged at slightly different times, and when combined with the movement of an airplane, results in this streaky red-green-blue pattern in the composite image.

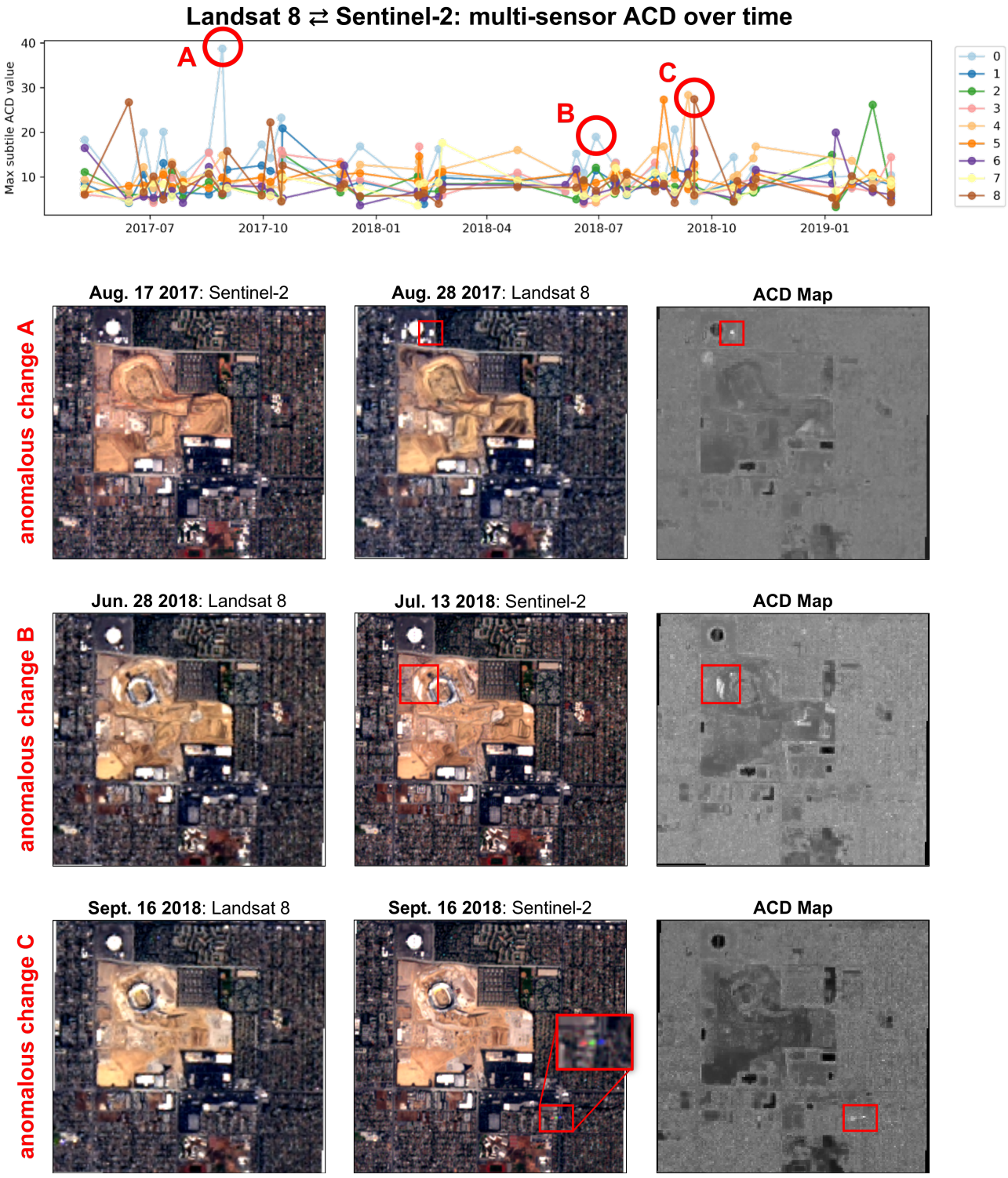


Figure 5. Tracked statistics for the nine subtiles over time between Landsat 8 and Sentinel-2. Three high-value anomalous changes are highlighted (anomalous change A, B, and C). The corresponding image pairs and ACD maps are provided.

### 4.2 SAR to MSI: Sentinel-1 and Sentinel-2

The results of our second experiment, where we compared changes from Dec. 2015 to Mar. 2019 for both MSI to MSI image pairs and SAR to MSI image pairs, are shown in Fig. 6. The first map in (a) corresponds to the MSI to MSI anomalous changes, and the second map in (b) corresponds to the SAR to MSI anomalous changes; for each, white indicates an anomalous change while gray and black indicate no change. In fact, it is often the case that black corresponds to pixels that are anomalous but not anomalously changed. The yellow box outlines the area surrounding the construction site.

In Fig. 6(c), we show the normalized difference of the two maps in order to compare their results. This difference map is scaled such that white indicates agreement between the maps in (a) and (b), blue indicates that the MSI→MSI change was greater than the SAR→MSI change, and red indicates that the SAR→MSI change was greater than the MSI→MSI change. We generally see agreement over the construction site, and also see a number of areas whose change is more anomalous in one image pair over the other. This is not surprising, as the construction site likely has surface changes that are not material changes (*e.g.*, growing piles of dirt), or spectral changes that are not significant surface changes (*e.g.*, laying out tarps). One area that stood out more prominently is the L-shaped region in blue at the bottom of the yellow annotated box in Fig. 6(c). This is a sharp feature that is a much larger anomalous change in the MSI→MSI change map.

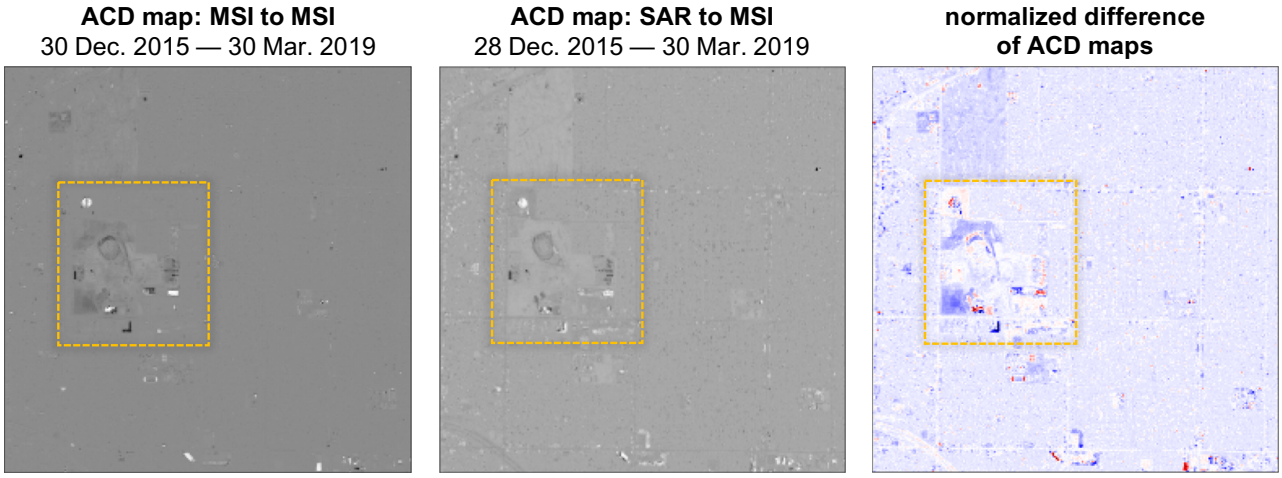


(a) (b) (c)

Figure 6. Comparison of detection maps. For the change maps in (a,b), white indicates anomalous change, while gray to black indicates no change (black often corresponds to pixels which are anomalous but not anomalously changed). For the difference map in (c), red indicates that MSI→MSI change was greater than SAR→MSI, blue indicates that the SAR→MSI change was more prominent, and white indicates that the same change (or lack of change) was observed in both scenarios.

In Fig. 7, we show further exploration on the L-shaped anomalous change that was more evident in the MSI→MSI detection map. To gain a better (and higher resolution) understanding of the nature of this change, we used Google Earth to look at historical imagery around the construction site before and during the image time frame. Because the analyzed image dates are from Dec. 2015 to Mar. 2019, we looked to prior imagery to see what was already present in that area. We can see that in Apr. 2014 there was a building already present and that it had a brown roof. Further exploration of additional historical layers shows us that the roof was unchanged as of Feb. 2016, was undergoing replacement to a white roof in Oct. 2016 and Apr. 2017, and was a fully white roof by Oct. 2017. This roof change occurs squarely within the time frame of the analyzed Sentinel-1 and Sentinel-2 imagery. What we can see from this higher-resolution historical imagery is that the building undergoes a material change but *not* a dramatic surface change. In other words, this is a change that would present itself in the MSI→MSI analysis, but not as strongly in the SAR→MSI data.

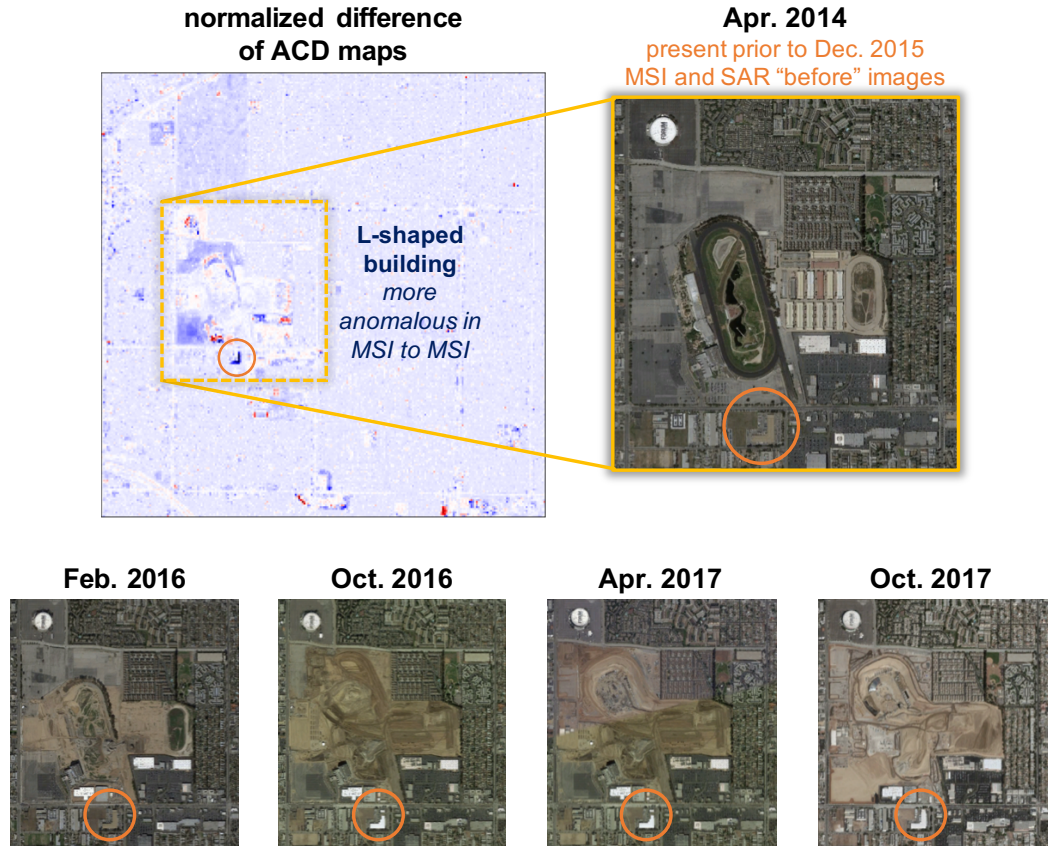


Figure 7. Exploration of the anomalous change corresponding to the L-shaped building. This change presents more strongly in the MSI→MSI because it is a significant material change, but not a strong surface change. Google Earth historical imagery shows that the roof was replaced within the time frame of the before and after images used in this analysis.

## 5. CONCLUSIONS AND FUTURE WORK

Because distribution-based anomalous change detectors do not involve image subtraction, and therefore do not require that images be spectrally aligned, we can use this class of change detector on disparate multispectral sensors as well as other phenomenologies. We applied the hyperbolic anomalous change detection (HACD) algorithm to satellite images taken from Landsat 8, Sentinel-2, and Sentinel-1. Landsat 8 and Sentinel-2 are both electro-optical multispectral imagers, though they have different numbers of bands and their wavelength bands do not line up. Sentinel-1 is a SAR imager, and those SAR images are phenomenologically quite different from the multispectral images in the optical domain. Although the results are qualitative, we did find that multi-sensor (and multi-modal) ACD was able to identify interesting changes. In the future, we will apply this approach to ground-truthed data from disparate sensors. The changes investigated here were taken from temporally adjacent pairs of images; since we in fact have a long time series of changes, we will also adapt our future analysis to take advantage of that opportunity. In particular, we will seek to classify changes by their temporal as well as their spectral signatures through using multi-dimensional joint distributions, distinguishing for instance among fleeting, recurring, and persistent changes.

## 6. ACKNOWLEDGMENTS

The research described in this paper was supported by the Los Alamos Laboratory Directed Research and Development (LDRD) program. We also thank Descartes Labs for supporting streamlined imagery access.

## REFERENCES


[1] Zelinski, M. E., Henderson, J., and Smith, M., "Use of Landsat 5 for change detection at 1998 Indian and Pakistani nuclear test sites," *IEEE J. Selected Topics in Applied Earth Obs. and Remote Sensing* **7**, 3453–3460 (Aug. 2014).

[2] Zelinski, M. E., Henderson, J. R., and Held, E. L., "Image registration and change detection for artifact detection in remote sensing imagery," *Proc. SPIE* **10644**, 1064413 (May 2018).

[3] Ziemann, A., Messinger, D. W., and Basener, B., "Iterative convex hull volume estimation in hyperspectral imagery for change detection," *Proc. SPIE* **7695** (2010).

[4] Schaum, A. and Stocker, A., "Long-interval chronochrome target detection," *Proc. Int. Symposium on Spectral Sensing Research* (1997).

[5] Nielsen, A. A., Conradsen, K., and Simpson, J. J., "Multivariate Alteration Detection (MAD) and MAF postprocessing in multispectral, bitemporal image data: New approaches to change detection studies," *Remote Sensing of Environment* **64**, 1–19 (1998).

[6] Carlotto, M. J., "Nonlinear background estimation and change detection for wide area search," *Optical Engineering* **39**, 1223–1229 (May 2000).

[7] Schaum, A. and Stocker, A., "Hyperspectral change detection and supervised matched filtering based on covariance equalization," *Proc. SPIE* **5425**, 77–90 (2004).

[8] Eismann, M., "Strategies for hyperspectral target detection in complex background environments," in [*Proc. Aerospace Conference*], IEEE (March 2006).

[9] Theiler, J., "Quantitative comparison of quadratic covariance-based anomalous change detectors," *Applied Optics* **47**(28), 12–26 (2008).

[10] Theiler, J. and Ziemann, A. K., "Right spectrum in the wrong place: a framework for local hyperspectral anomaly detection," *Proc. Computational Imaging XIV* (2016).

[11] Acito, N., Diani, M., Corsini, G., and Resta, S., "Introductory view of anomalous change detection in hyperspectral images within a theoretical gaussian framework," *IEEE Aerospace and Electronic Systems Magazine* **32**, 2–27 (Sept. 2017).

[12] Stein, D. W. J., Beaven, S. G., Hoff, L. E., Winter, E. M., Schaum, A. P., and Stocker, A. D., "Anomaly detection from hyperspectral imagery," *IEEE Signal Processing Magazine* **19**, 58–69 (Jan 2002).

[13] Theiler, J. and Cai, D. M., "Resampling approach for anomaly detection in multispectral images," *Proc. SPIE* **5093**, 230–240 (2003).

[14] Adler-Golden, S. M., "Improved hyperspectral anomaly detection in heavy-tailed backgrounds," *Proc. IEEE Workshop on Hyperspectral Image and Signal Processing: Evolution in Remote Sensing (WHISPERS)* **1** (2009).

[15] Matteoli, S., Diani, M., and Corsini, G., "A tutorial overview of anomaly detection in hyperspectral images," *IEEE A&E Systems Magazine* **25**, 5–27 (2010).

[16] Theiler, J., [*Anomaly Testing: Chapter 19 in Statistical Methods for Materials Science: The Data Science of Microstructure Characterization*], 323–338, CRC Press (2019).

[17] Malila, W. A., "Change vector analysis: an approach for detecting forest changes with Landsat," *Proc. IEEE Symposium on Machine Processing of Remotely Sensed Data* , 326–335 (1980).

[18] Johnson, R. D. and Kasischke, E. S., "Change vector analysis: a technique for multispectral monitoring of land cover and condition," *Int. J. Remote Sensing* **19**, 411–426 (Jan. 1998).

[19] Bruzzone, L. and Prieto, D. F., "Automatic analysis of the difference image for unsupervised change detection," *IEEE Trans. Geoscience and Remote Sensing* **38**, 1171–1182 (2000).

[20] Bovolo, F. and Bruzzone, L., "A theoretical framework for unsupervised change detection based on change vector analysis in the polar domain," *IEEE Trans. on Geoscience and Remote Sensing* **45**(1), 218–236 (2007).

[21] Meola, J., Eismann, M. T., Moses, R. L., and Ash, J. N., "Detecting changes in hyperspectral imagery using a model-based approach," *IEEE Trans. on Geoscience and Remote Sensing* **49**, 2647–2661 (July 2011).

[22] Meola, J., Eismann, M. T., Moses, R. L., and Ash, J. N., "Application of model-based change detection to airborne VNIR/SWIR hyperspectral imagery," *IEEE Trans. on Geoscience and Remote Sensing* **50**, 3693–3706 (Oct. 2012).

[23] Schaum, A. and Stocker, A., "Spectrally selective target detection," *Proc. Int. Symposium on Spectral Sensing Research* (1997).

[24] Stocker, A. and Villeneuve, P., "Generalized chromodynamic detection," *Proc. IEEE IGARSS* , 1–4 (July 2008).

[25] Theiler, J. and Perkins, S., "Proposed framework for anomalous change detection," *Proc. 23rd Int. Conference on Machine Learning (ICML)* (2006).

[26] Theiler, J., Scovel, C., Wohlberg, B., and Foy, B. R., "Elliptically-contoured distributions for anomalous change detection in hyperspectral imagery," *IEEE Geoscience and Remote Sensing Letters* **7**(2), 271–275 (2010).

[27] Theiler, J., Foy, B. R., Wohlberg, B., and Scovel, C., "Parametric probability distributions for anomalous change detection," *Proc. Military Sensing Symposia (MSS)* (2010).

[28] Longbotham, N. and Camps-Valls, G., "A familly of kernel anomaly change detectors," *Proc. IEEE WHISPERS* (2014).

[29] Theiler, J., "Spatio-spectral anomalous change detection in hyperspectral imagery," *Proc. IEEE Global Conference on Signal and Information Processing* (2013).

[30] Schaum, A. P. and Stocker, A. D., "Subclutter target detection using sequences of thermal infrared multispectral imagery," *Proc. SPIE* **3071**, 12–22 (Aug. 1997).

[31] Theiler, J. and Adler-Golden, S. M., "Detection of ephemeral changes in sequences of images," *Proc. 37th IEEE Applied Imagery Pattern Recognition Workshop (AIPR)* (October 2008).

[32] Theiler, J. and Wohlberg, B., "Local co-registration adjustment for anomalous change detection," *IEEE Trans. on Geoscience and Remote Sensing* **50**, 3107–3116 (August 2012).

[33] Vongsy, K., Eismann, M. T., and Mendenhall, M. J., "Extension of the linear chromodynamics model for spectral change detection in the presence of residual spatial misregistration," *IEEE Trans. on Geoscience and Remote Sensing* **53**, 3005–3021 (June 2015).

[34] Fenno, N. and Farmer, S., "Los Angeles Rams break ground on $2.6-billion Inglewood stadium, 'new era' of NFL," *Los Angeles Times* (Nov. 2016).

[35] European Space Agency (ESA), "Sentinel Online." `https://sentinel.esa.int/`.

[36] United States Geological Survey (USGS), "Landsat Missions." `https://www.usgs.gov/landsat`.

[37] "2017 MTV Video Music Awards." Wikipedia [online]: `https://en.wikipedia.org/wiki/2017_MTV_Video_Music_Awards`.